College of Earth and Mineral Sciences

PENNSTATE

DEPARTMENT OF MATERIALS SCIENCE

METALLURGY PROGRAM

ANNUAL TECHNICAL REPORT

January 1989

Contract No. N00014-84-k-0201

ANALYSIS OF HYDROGEN EVOLUTION AND ENTRY INTO METALS
FOR THE DISCHARGE-RECOMBINATION PROCESS

H. W. Pickering

Department of Materials Science and Engineering
The Pennsylvania State University

89   2   21   075

PENN STATE
College of Earth and Mineral Sciences

Undergraduate Majors

Ceramic Science and Engineering, Fuel Science, Metals Science and Engineering, Polymer Science;
Mineral Economics; Mining Engineering, Petroleum and Natural Gas Engineering;
Earth Sciences, Geosciences; Geography; Meteorology.

Graduate Programs and Fields of Research

Ceramic Science and Engineering, Fuel Science, Metals Science and Engineering, Polymer Science;
Mineral Economics; Mining Engineering, Mineral Processing, Petroleum and Natural Gas
Engineering;
Geochemistry and Mineralogy, Geology, Geophysics; Geography; Meteorology.

Universitywide Interdisciplinary Graduate Programs Involving EMS Faculty and Students

Earth Sciences, Ecology, Environmental Pollution Control Engineering, Mineral Engineering
Management, Solid State Science.

Associate Degree Programs

Metallurgical Engineering Technology (Shenango Valley Campus).

Interdisciplinary Research Groups Centered in the College

C. Drew Stahl Center for Advanced Oil Recovery, Center for Advanced Materials, Coal Research
Section, Earth System Science Center, Mining and Mineral Resources Research Institute, Ore
Deposits Research Group.

Analytical and Characterization Laboratories (Mineral Constitution Laboratories)

Services available include: classical chemical analysis of metals and silicate and carbonate rocks;
X-ray diffraction and fluorescence; electron microscopy and diffraction; electron microprobe
analysis; atomic absorption analysis; spectrochemical analysis; surface analysis by secondary ion
mass spectrometry (SIMS); and scanning electron microscopy (SEM).

ADA204906

REPORT DOCUMENTATION PAGE		READ INSTRUCTIONS BEFORE COMPLETING FORM
1. REPORT NUMBER	2. GOVT ACCESSION NO.	3. RECIPIENT'S CATALOG NUMBER
4. TITLE (and Subtitle) Analysis of Hydrogen Evolution and Entry Into Metals for the Discharge Recombination Process		5. TYPE OF REPORT & PERIOD COVERED Annual Technical Report
		6. PERFORMING ORG. REPORT NUMBER
7. AUTHOR(s) Howard W. Pickering		8. CONTRACT OR GRANT NUMBER(s) N00014-84-k-0201
9. PERFORMING ORGANIZATION NAME AND ADDRESS The Pennsylvania State University		10. PROGRAM ELEMENT, PROJECT, TASK AREA & WORK UNIT NUMBERS
11. CONTROLLING OFFICE NAME AND ADDRESS		12. REPORT DATE January 1989
		13. NUMBER OF PAGES
14. MONITORING AGENCY NAME & ADDRESS(if different from Controlling Office)		15. SECURITY CLASS. (of this report)
		15a. DECLASSIFICATION/DOWNGRADING SCHEDULE

16. DISTRIBUTION STATEMENT (of this Report)

17. DISTRIBUTION STATEMENT (of the abstract entered in Block 20, if different from Report)

18. SUPPLEMENTARY NOTES

19. KEY WORDS (Continue on reverse side if necessary and identify by block number)

20. ABSTRACT (Continue on reverse side if necessary and identify by block number)

A mechanistic model has been developed which for the first time considers the effect of hydrogen entry into a metal on the kinetics of the hydrogen evolution reaction (h.e.r.). The model enables computation of (i) the hydrogen surface coverage and surface concentration, (ii) the hydrogen adsorption, absorption, discharge and recombination rate constants, and (iii) the h.e.r. coverage-dependent transfer coefficient, α, and the exchange current density i_o, from a knowledge of the steady state hydrogen permeation current, cathodic charging current, hydrogen overvoltage and hydrogen

DD FORM 1473 EDITION OF 1 NOV 65 IS OBSOLETE
1 JAN 73
S/N 0102-LF-014-6601

(#20 continued)

diffusivity. The model predicts a linear relationship between permeation flux and square-root of the hydrogen recombination flux and provides an analytical method to determine the cathodic potential range for operation of a coupled discharge-recombination mechanism of the h.e.r. With modifications the model can treat permeation data for which (i) the mechanics of the discharge step involve a (proposed) selvedge reaction and (ii) surface hydrogen coverages are relatively high as in the presence of poisons (e.g., H_2S or As_2O_3). Some of the existing literature data for hydrogen permeation in iron and nickel in acid and alkaline solutions are successfully analyzed.

Accesion For	
NTIS CRA&I	☑
DTIC TAB	☐
Unannounced	☐
Justification	
By *per HP*	
Distribution /	
Availability Codes	

Dist	Avail and / or Special
A-1	

ANALYSIS OF HYDROGEN EVOLUTION AND ENTRY INTO METALS FOR THE DISCHARGE-RECOMBINATION PROCESS

Rajan N. Iyer, and Howard W. Pickering
Department of Materials Science and Engineering
The Pennsylvania State University
University Park, PA   16802

and

Mehrooz Zamanzadeh
Professional Service Industries - PTL Division
850 Poplar Street
Pittsburgh, PA   15220

ABSTRACT

A mechanistic model has been developed which for the first time considers the effect of hydrogen entry into a metal on the kinetics of the hydrogen evolution reaction (h.e.r.). The model enables computation of (i) the hydrogen surface coverage and surface concentration; (ii) the hydrogen adsorption, absorption, discharge and recombination rate constants; and (iii) the h.e.r. coverage-dependent transfer coefficient, α, and the exchange current density i_o, from a knowledge of the steady state hydrogen permeation current, cathodic charging current, hydrogen overvoltage and hydrogen diffusivity. The model predicts a linear relationship between permeation flux and square-root of the hydrogen recombination flux and provides an analytical method to determine the cathodic potential range for operation of a coupled discharge-recombination mechanism of the h.e.r. With modifications the model can treat permeation data for which (i) the mechanics of the discharge step involve a (proposed) selvedge reaction and (ii) surface hydrogen coverages are relatively high as in the presence of poisons (e.g., H_2S or $As_2 O_3$). Some of the existing literature data for hydrogen permeation in iron and nickel in acid and alkaline solutions are successfully analyzed.

INTRODUCTION

Hydrogen is one of the most damaging species in metals, causing hydrogen assisted cracking, blisters, etc. Hydrogen entry into metals from aqueous solutions has been studied extensively by hydrogen permeation experiments of thin samples using the Devanathan-Stachurski cell[1-7]. Some studies carried out on iron in acid and alkaline solutions[2,4,6] reveal a coupled discharge-recombination mechanism for the hydrogen evolution reaction (h.e.r.) with diffusion of absorbed hydrogen into the metal being rate controlling for the permeation process. The models based on this mechanism predict a square-root relationship between the hydrogen charging current and the steady state hydrogen permeation flux or current[2]. In all of these models, it has been assumed that the hydrogen permeation flux is negligible. It has also been assumed that the hydrogen coverage (θ) is quite low, although the coverage itself is unknown. However, especially when poisons such as H_2S or As_2O_3 are present in the solution, both the permeation current and the hydrogen coverage can be appreciable[8,9]. If the steady state permeation current (i_∞) is proportional to the square-root of the charging current (and the Tafel slope is -120 mV decade^{-1} and $d\eta/d\log i_\infty$ is -240 mV decade^{-1} where η is the overpotential for the h.e.r.), the h.e.r. is generally considered to follow a coupled discharge-recombination mechanism. Apart from these considerations which have not produced operative models yielding the relevant parameters, e.g., θ, the current models also do not explain the mechanics of the intermediate reaction between adsorption and absorption of hydrogen in metals, which is probably correctly assumed in many cases, but perhaps not in all, to be in equilibrium at the cathode surface.

The thrust of this paper is to develop a novel model for the electrochemical reactions involving hydrogen evolution and permeation, enabling calculation of the rate constants and hydrogen coverages for the first time using data obtained from hydrogen permeation experiments. In this model, the effect of hydrogen permeation on the h.e.r. is taken into

account and an analytical method is developed to check the operating mechanism of the h.e.r. The model is tested using literature data from hydrogen permeation experiments.

THEORETICAL

I. Development of the Basic Model

The charge transfer (hydrogen discharge) reaction can be represented by

$$H_3O^+ + e^- + M = MH_{ads} + H_2O$$
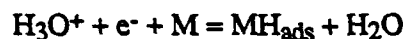
and is followed by two reactions, which are hydrogen desorption (or chemical recombination: $2 H_{ads} \rightarrow H_2$) and hydrogen absorption (permeation) into the metal. In order for these latter two reactions to take place, an intermediate adsorption-absorption step is involved[10,11]. A quantitative derivation of the relationships between hydrogen surface coverage, rate constants, transfer coefficient, etc. and hydrogen charging current, overpotential and permeation flux is presented below with the following conditions or assumptions:

(1)   Hydrogen discharge involves only a single electron transfer reaction and hydrogen evolution occurs by the chemical recombination reaction ($2 H_{ads} = H_2$). It is also assumed that $\eta \gg RT/F$ or that the recombination step is not rate determining so that the backward reaction (H oxidation) can be neglected. Also, Langmuir conditions are assumed for the hydrogen coverage in the development of the basic model in this paper, but the basic model can be modified to include other surface coverage conditions as described elsewhere[8].

(2)   The intermediate adsorption-absorption reaction is in local equilibrium.

(3) The permeation flux, i_∞ is described by a simple diffusion of hydrogen through the metal membrane, with a finite concentration of hydrogen, c_s, at the charging surface and zero concentration at the exit (anodic) surface.

(4) $i_c = i_\infty + i_r$, where i_c = charging current density and i_r = steady state desorption flux or hydrogen recombination current density. In other words, only steady state conditions are considered when no further trapping will occur, since all the traps for hydrogen in the metal will be saturated by the end of the transient stage of hydrogen permeation. This assumption of steady state allows calculation of i_r from the measured i_c and i_∞ values in hydrogen permeation experiments.

From the first assumption the backward reaction of the h.e.r. is negligible and thus the charging current is

$$i_c = Fk_1^O a_{H^+} e^{-\alpha E^{eq} F/RT} (1-\theta_s)e^{-\alpha\eta F/RT} = Fk_1(1-\theta_s)e^{-a\alpha\eta} = i_o'(1-\theta_s)e^{-a\alpha\eta} \qquad (1)$$

where k_1^O = the rate constant for the forward reaction; θ_s = the surface coverage by hydrogen; α = the transfer coefficient; a_{H^+} = the hydrogen ion activity; k_1 = the discharge rate coefficient = $k_1^O a_{H^+} e^{-a\alpha E^{eq}}$; E^{eq} = the equilibrium potential for the h.e.r.; i_o' = Fk_1; i_o = the exchange current density = $i_o'(1-\theta_e)$; θ_e = the hydrogen surface coverage at equilibrium; and $a = F/RT = 38.94$ V^{-1} at $T = 300°K$.

Using Assumption (1), the steady state desorption flux (hydrogen recombination current) is given by:

$$i_r = Fk_3\theta_s^2 \qquad (2)$$

where k_3 = the recombination rate constant. Using Assumption (3), the steady state permeation flux or current is given by:

$$i_\infty \approx F(D_1/L)\, c_s \tag{3}$$

where D_1 = the bulk diffusivity of hydrogen in the metal, L = the thickness of the metal membrane, and c_s = the concentration of hydrogen in the metal adjacent to the surface.

From Equation (3),

$$c_s = \left(\frac{L}{FD_1}\right) i_\infty = b i_\infty \tag{3a}$$

where $b = L/(FD_1)$.

Considering the intermediate reaction of hydrogen absorption and adsorption, along with Assumption (2), the net rate of hydrogen entry (i_∞) is also given by[10,11]: $i_\infty = F(k_{abs}\theta_s - k_{ads}c_s)$. Substituting for i_∞ from Equation (3) and rearranging, one obtains

$$\theta_s = \frac{\left[k_{ads} + \left(\dfrac{D_1}{L}\right)\right]}{k_{abs}} c_s = c_s/k'' \tag{4}$$

where

$$k'' = \frac{k_{abs}}{\left[k_{ads} + \dfrac{D_1}{L}\right]} \tag{4a}$$

If $\dfrac{D_1}{L} \ll k_{ads}$, then $k'' = \dfrac{k_{abs}}{k_{ads}} = k'$, where k' is usually called the equilibrium absorption-adsorption constant. It will be shown later that the assumption that the absorption-adsorption constant is thickness independent, i.e., it is the same as k', can be valid for thick membranes or low values of D_1. From Equations (2), (3) and (4),

$$i_{\infty} = k'' \left(b\sqrt{Fk_3} \right)^{-1} \sqrt{i_r} \tag{5}$$

Equation (5) predicts that the hydrogen permeation flux (i_{∞}) will have a square-root relationship with the hydrogen evolution (recombination) current, i_r, where $i_r = i_c - i_{\infty}$ from Assumption (4). This relationship has been experimentally observed by Dafft et al.[9]. In the special case, when $i_{\infty} << i_r$ (ie. $i_c \cong i_r$), Equation (5) reduces to i_{∞} being proportional to $\sqrt{i_c}$, i.e., the Bockris et al.[2] model.

The Tafel slope for the h.e.r. and $\dfrac{d\eta}{d\log i_{\infty}}$ are calculated for this model. From Equation (5),

$$i_{\infty} = K\, i_r^{1/2} = K \left(i_c - i_{\infty} \right)^{1/2} \tag{5a}$$

where K is a constant.

Taking logarithms of Equation (5a) and differentiating with respect to η,

$$\frac{d\ln(i_{\infty})}{d\eta} = \frac{1}{2}\frac{d\ln(i_c)}{d\eta} + \frac{1}{2}\frac{d\ln\left(1 - \frac{i_{\infty}}{i_c}\right)}{d\eta} \tag{5b}$$

Since the second term on the right hand side of Equation (5b) is equivalent to

$$\frac{i_{\infty}/i_c}{2(1 - i_{\infty}/i_c)}\left(\frac{d\ln i_c}{d\eta} - \frac{d\ln i_{\infty}}{d\eta} \right),\quad \text{Equation (5b) becomes}$$

$$\frac{d\eta}{d\log i_{\infty}} = \left(2 - \frac{i_{\infty}}{i_c} \right)\frac{d\eta}{d\log i_c} \tag{5c}$$

When $i_{\infty} << i_c$

$$s_{\infty t} = 2\, s_{ct} \tag{5d}$$

where $s_{\infty t} = \dfrac{d\eta}{d\log i_\infty}$ and $s_{ct} = \dfrac{d\eta}{d\log i_c}$.

For example, when $\alpha = 0.5$ and $\theta \sim 0$, $s_{ct} = -120$ mV decade^{-1} (since from Equation (1), $\dfrac{d\eta}{d\log i_c} = -\dfrac{2.303}{a\alpha}$) and so $s_{\infty t} = -240$ mV decade^{-1}, which is in exact agreement with previous models and findings. However, if $i_\infty \approx i_c$, Equation (5c) yields $s_{\infty t} = -120$ mV decade^{-1} for $s_{ct} = -120$ mV decade^{-1}. Thus, in general, the following inequality will hold for $\dfrac{d\eta}{d\log i_\infty}$:

$$\left|\frac{d\eta}{d\log i_c}\right| < \left|\frac{d\eta}{d\log i_\infty}\right| < 2\left|\frac{d\eta}{d\log i_c}\right| \tag{5e}$$

It may be additionally noted from Equation (5c) that for significant hydrogen permeation (i_∞), either the Tafel slope or $d\eta/d\log i_\infty$ or both will vary as a consequence of the dependence of θ on η implicit in Equation (5). Many data relating to hydrogen permeation including those of Bockris et al.[2], Kato et al.[3] and Dafft et al.[9] clearly show the nonconstant behavior of these quantities. It will be cautioned here that an increase in i_∞/i_c corresponds to an increase in θ_s in which case the Frumkin-Temkin correction may need to be applied for i_c and i_r in Equations (1) and (2). This will be discussed towards the end of this analysis.

In order to find the values of k'', k_3 and i_0', analysis of the η-i_c-i_∞ data has to be carried out. Rearranging Equation (1),

$$\theta_s = 1 - \frac{i_c\, e^{a\alpha\eta}}{i_0'} \tag{6}$$

Equation (6) can be called the polarized adsorption isotherm. This is to be contrasted with the Langmuir adsorption isotherm which is good only if at least quasi-equilibrium exists so that the forward and the reverse currents are equal. On the other hand, Equation (6) gives

the adsorption isotherm (i.e. surface coverage) for a non-reversible reaction, such as when the nonreversible reaction is coupled to a subsequent reaction. Also from Equations (3a) and (4),

$$\theta_s = \frac{bi_\infty}{k''} \tag{6a}$$

Equation (6a) can be called the polarized adsorption-absorption isotherm. By differentiating Equation (6a) with respect to i_∞,

$$\frac{\partial \theta_s}{\partial i_\infty} = \frac{b}{k''} \tag{6b}$$

Equation (6b) tells us that the gradient of the polarized adsorption isotherm (ie. the polarized coverage) with the absorption (or permeation) current will yield the thickness dependent absorption-adsorption constant, k''. However, in practice, θ_s is not known. So one has to eliminate θ_s between Equations (6) and (6a), in order to obtain the following relationship:

$$i_c = i_0' \ [1 - (bi_\infty/k'')]e^{-a\alpha\eta} \tag{6c}$$

i.e.,

$$i_c e^{a\alpha\eta} = -(bi_0'/k'') \ (i_\infty) + i_0' \tag{6d}$$

Equation (6d) predicts that a linear relationship should be obtained between i_∞ and $f_{i\eta} = (i_c e^{a\alpha\eta})$ where α is obtained by the procedure shown in the Appendix, and the value of the bulk hydrogen diffusivity, D_l, in the constant, b, is separately obtained from other (transient) permeation measurements or from the literature. Thus, Equation (6d) enables direct evaluation of k'' (from the slope of $f_{i\eta}$ vs i_∞ where i_0' is the intercept at $i_\infty = 0$). Now, having k'', the hydrogen surface coverage θ_s can be obtained from Equation (6a), and k_3 can be obtained from Equation (5).

Thus, Equation (6c) or (6d) quantitatively illustrates the effect of i_∞ on the h.e.r. The effect of neglecting i_∞ is to eliminate k'' in equation (6d) so that one only obtains the value of i_0'.

Thus, once α is determined, k'', k_3 and i_0' can be determined by regression analysis of Equations (5) and (6d), if the plots of i_∞ vs $\sqrt{i_r}$ (Equation (5)) and $f_{i\eta}$ vs i_∞ (Equation (6d)) are linear. An absence of linearity in the experimentally determined plots of Equations (5) and (6d) would be an indication that at least one of the three assumptions mentioned above is not met, e.g., steady state was not achieved in the experiments, the backward reaction of the discharge step is significant or the discharge-recombination process is not operating. Finally, from the measured values of i_c and η, θ_s vs η can be plotted using Equation (6). The equilibrium surface coverage of hydrogen (θ_e) can be determined by extrapolating this plot to $\eta = 0$. Then, from Equation (1)

$$k_1 = i_0''/F \tag{7}$$

$$k_1^o = k_1 / \left(a_{H^+} e^{-\alpha E^{eq} F/RT} \right) \tag{7a}$$

and

$$i_0 = i_0' (1 - \theta_e) \tag{8}$$

Comparison of the discharge rate constant and the recombination rate constant can provide some insight into the reaction mechanism. The discharge reaction rate is potential dependent, i.e., as the cathodic overvoltage (η) is increased, the potential dependent reaction rate constant ($k_{1\eta}$) will be increased; whereas, the recombination reaction rate constant depends solely on physico-chemical processes, e.g., the surface diffusion of H_{ad} atoms. Thus, it is obvious that the potential range has to be considered in order to compare these rate constants for mechanistic analysis. From Equation (1) the potential dependence of $k_{1\eta}$ may be taken to be of the form,

$$k_{1\eta} = k_1 e^{-a\alpha\eta} \qquad (9)$$

One of the most common mechanisms of the hydrogen evolution reaction on iron is the coupled discharge-recombination mechanism. It is considered that an overall process is coupled if the energies of the activated states of more than one step are within 1 to 2 kcal/mole with respect to their initial states[12]. Since the rate, v_i, is proportional to $e^{-(\Delta G_i^*/RT)}$ (ΔG_i^* being the activated energy of reaction i), the discharge and recombination reactions can be considered to be coupled if $v_1/v_3 = (e^{-\Delta G_1^*/RT}) / (e^{-\Delta G_3^*/RT}) = e^{-(\Delta G_1^* - \Delta G_3^*)/RT} = e^{\pm 1500/600} \approx 12$ or $1/12$. Therefore, if v_1 and v_3 are within one order of magnitude of each other, then,

$$0.1\,k_3 < k_{1\eta} < 10\,k_3 \qquad (10)$$

and the hydrogen discharge and recombination reactions will be coupled.

Equation (10) can be utilized to estimate the potential range where the reaction will occur by a coupled discharge-recombination mechanism. From Equations (9) and (10), the lower limit of the potential range (η_c^1) is given by:

$$\eta_c^1 = [\ln(10\,k_1/k_3)]/a\alpha \qquad (11a)$$

and the upper limit of the potential range (η_c^u) is given by:

$$\eta_c^u = \left[\ln\left(k_1/(10\,k_3)\right) \right]/a\alpha \qquad (11b)$$

Thus, conditions under which a coupled discharge recombination mechanism operates are that $k_3 \sim k_{1\eta}$ and i_∞ vs $\sqrt{i_r}$ and $f_{1\eta}$ vs i_∞ are linear. These plots provide a convenient check of the mechanism since if either plot is nonlinear a coupled discharge-recombination mechanism is ruled out.

The basic model developed here will be known as the I-P-Z model, in future references. Although this model was developed considering acid solutions, similar relationships will be valid for alkaline solutions. The main difference will be that a_{H+}

in Equation (1) will have to be replaced by a_{H_2O} ($\cong 1$) and hence

$i_o{}' = Fk_1^O a_{H_2O} e^{-\alpha E^{eq}F/RT} = F k_1^O e^{-\alpha E^{eq}F/RT}$. Also, $k_1 = k_1^O a_{H^+} e^{-\alpha E^{eq}F/RT}$ in Equations (9) through (11) will be replaced simply by $k_1 = k_1^O e^{-\alpha E^{eq}F/RT}$.

Another important modification to be stressed here is the correction to be applied when θ is larger than ~0.1, as pointed out earlier. In the above derivation of the basic model, for simplicity sake, Langmuir conditions[4,13] were considered. But deviations will occur when θ_s is significant and so i_c and i_r have to be corrected by utilizing the Frumkin-Temkin relationship[13] for the hydrogen coverage function. Then Equations (1) and (2) become

$$i_c = i_o''\left(1 - \theta_s\right) e^{-\gamma\theta_s/RT} e^{-\alpha\alpha\eta} \qquad (12)$$

$$i_r = F k_3 \theta_s^2 e^{2\gamma\theta_s/RT} \qquad (13)$$

Here γ refers to the rate of change of the apparent standard free energy of adsorption with coverage[13]. Modifications of the basic model given above using Eqs. (12) and (13) are presented elsewhere[8,14].

The question as to whether or not the intermediate reaction, termed the absorption-adsorption reaction, is actually in local equilibrium under all circumstances needs also to be critically examined. This seems especially true in the absence of any direct experimental evidence on the question and in light of the fact that very high fugacities can be involved under cathodic polarization of the electrode[15-17]. This point is addressed below in the Discussion.

RESULTS AND DISCUSSION

I. **Data Analysis Using the Basic I-P-Z Model.**

The basic I-P-Z model developed above is tested for various literature data[2,3,6,18] of hydrogen permeation experiments on iron of different purity and zone-refined (99.995 wt %) nickel. Figures 1 and 2 show the plots of $\log(i_c)$ vs η and $\log(i_\infty)$ vs η for these cases. It is clear that the plots are linear and, hence, the quadratic equation in α (Equation (A.5) in the Appendix) is easily solved for each of the cases, and these α values are given in Table I.

Figure 3 shows the i_∞ vs $\sqrt{i_r}$ plots, which are all linear as confirmed by various statistical tests. Three of the plots pass through or close to the origin and one has a relatively large non-zero (positive) intercept. By performing various statistical analyses, including the Student's t Test[19], it has been confirmed that the non-zero (positive) intercept, for the data of Bockris et al.[2], is significant at 95% or even at 99% confidence levels. The basic I-P-Z model is strictly valid, however, only for plots that pass through the origin. Therefore, for the three cases in Figure 3 where the i_∞ vs $\sqrt{i_r}$ plots are linear and pass through the origin, the basic I-P-Z model is applicable and so $i_c a^{\alpha \eta}$ versus i_∞ (Equation (6d)) can be plotted. Figure 4 shows these plots, which are seen to be linear, confirming the assumption of steady state [i.e., Assumption (4)]. But due to the extremely small values of i_0', the slopes in Fig. 4 are quite small making the lines seem almost horizontal. For the plot in Fig. 3 with the non-zero intercept, modification of the basic I-P-Z model is necessary and this is presented in Section II.

Since the plots in Figs. 3 and 4 are linear, all of the constants k_3, i_0', k'', k_1^0 and θ_e are determined for the data in References 3, 6 and 18 from the regression analysis of Equations (5) and (6d). A value of $D_1 = 5 \times 10^{-5}$ cm^2 s^{-1} was used for iron in these analyses although measurements of the true lattice hydrogen diffusivity in iron are not easily made as shown by the great variation in measured values[20]. For nickel, $D_1 = 4 \times 10^{-10}$ cm^2 s^{-1}[18] was used. All of these values are tabulated in Table I.

The accuracy levels of the computed values of the transport and kinetic constants and coefficients in Table I are primarily limited by the accuracy of the diffusivity and the α values. These results were confirmed by various statistical analyses (including the F test and the Student's t test) in that the confidence levels of the estimated parameters, (i.e., slopes and intercepts), from the regression analyses of Equations (5) and (6d), were better than that possible for the diffusivity and α values. Even a slight error in α can cause a large scatter in the $i_c e^{a\alpha\eta}$ vs η plot, since α appears in the exponential term.

Since k'' is known, θ_S values are obtained by using Equation (6a) for various i_∞ (or equivalently η) values. θ_S vs η plots are given in Figure 5, which shows that the hydrogen surface coverages are quite small in all of the cases, i.e., $\theta_S < 0.15$. Although only a few experimental determinations of θ_S exist in the literature, values for comparison with those in this paper for the 0.1 N H_2SO_4 solutions have yielded similar θ_S values, i.e., in the range of 0.01 to 0.1[10,21]. More (direct) experimental measurements of θ_S, however, are needed for checking the model.

As shown above, this model is able to determine the transfer coefficient α, as per Equation (A.5) of the Appendix and it is a function of both the inverse Tafel slope, s_c, and the slope (s_∞), $d\ln(i_\infty)/d\eta$. Table I shows that the α values fall on either side of 0.5 for the acid solutions with the data of Kato $et\ al.$[3] being the furthest from 0.5. It is to be noted that the different iron data were for samples having varying impurities, membrane thicknesses and pretreatments. The tendency for surface segregation (e.g., during prior heat treatment) is greater the less pure is the iron, and the tendency for impurity adsorption (from the electrolyte during the permeation experiment) is greater the thicker is the sample because of the longer permeation time. Kato $et\ al.$[3] used 99.98 wt % iron (0.004% C, 0.006% Si and 0.002% P, S and Al) membranes, 2mm thick and 0.1 N H_2SO_4 charging solution, and the charging surface was mechanically polished prior to the hydrogen charging experiment. Bockris $et\ al.$[2] used Armco iron (99.9 wt %) membranes, 0.77 mm thick, 0.1 N H_2SO_4 and the charging surface was etched as the final sample preparation

step. Zamanzadeh et al.[6] used Ferrovac E-iron (the most pure of the three) membranes, 0.365 mm thick, alkaline solution (0.1N NaOH) and the membranes were annealed at 1273 K in an argon back-filled evacuated apsu... In addition, the surface pH values were probably different for the three sets of data even for the 0.1N H_2SO_4 solutions in the absence of a buffer. Considering all of these aspects, it is not surprising to see the variability of the computed values for the three sets of iron data in Table I. From Equation (1), an explanation of why the i_0 values for iron are different in each case would be based on pH and factors affecting both k_1^o (such as impurity adsorption) and α.

Besides surface conditions such as the presence of oxide films, other factors, such as impurity adsorption, surface segregation and surface enrichment that is caused by selective dissolution, can change the kinetics of the surface reactions, including the absorption-adsorption step and hydrogen desorption. The effect of one or more of these factors could account for the variation of k" (besides the very important thickness effects, as described later) and k_3 (recombination constant) values for the iron data in Table 1.

As pointed out in the last section, the potential dependent discharge reaction rate coefficient $(k_{1\eta})$ depends on the overvoltage (η). At very low η values, the discharge reaction will be slower than the recombination reaction and at moderate to high overvoltages, they will be coupled. In general, for iron (refer to Table I) hydrogen charging at an overpotential between -400 and -900 mV will involve a coupled discharge-recombination mechanism. For nickel, this overpotential range is between -440 and -650 mV. However, the overpotentials employed in the experiments were smaller than these ranges (see Figures 1, 2, or 5), i.e., the overpotentials correspond to the discharge reaction being slower than or about as fast as the recombination reaction, consistent with the low values of θ_s in all of the cases (Fig. 5). These observations may provide a clue in understanding the mechanism in the familiar industrial problem of the enhancement of hydrogen permeation in the presence of poisons like H_2S, in that a reduction in k_3 (e.g., a reduction in surface diffusivity of H_{ad}) or increase in k_1^o or both can push the reaction towards a fully coupled mechanism. In this way,

due to the presence of poisons, such as H_2S, the hydrogen coverage is increased and since the hydrogen diffusivity is relatively high in iron, the hydrogen permeation is greatly enhanced. A more advanced study of these aspects in the case of enhanced hydrogen entry due to poisons is shown in the modified I-P-Z model[8,14] taking into account the Frumkin-Temkin corrections[13] for hydrogen coverage.

II. A Modified I-P-Z Model for Selvedge Reactions.

The fact that a statistically significant non-zero (positive) intercept was obtained in Figure 3, for the data of Bockris et al.[2], poses an interesting question: Is Assumption (2) valid in all cases, i.e., is the adsorption-absorption reaction in local equilibrium? As pointed out earlier, in the absence of any direct experimental evidence on the question and in the light of the fact that very high fugacities can be involved under cathodic polarization of the metal electrode[15-17] there is good reason to consider other possibilities for the intermediate reaction that follows the hydrogen discharge reaction. In terms of quantitatively treating hydrogen permeation data that contain positive or negative intercepts, it means considering other intermediate reactions that may themselves produce concentration profiles in the near surface or selvedge region that differ from the concentration profile in the bulk metal (established by the bulk diffusion of hydrogen). Three different possible cases of H concentration profiles are sketched in Figure 6.

Figure 6(a) depicts the assumed condition for the basic I-P-Z model, i.e., the condition of local equilibrium of the adsorption-absorption reaction. In this case i_∞ is proportional to $\sqrt{i_r}$, and the intercept (c_g) of the i_∞ vs $\sqrt{i_r}$ plot is zero. Furthermore, for equilibrium of the adsorption-absorption reaction, the physical situation is that the absorbed state is located in the very near vicinity of the adsorbed state, i.e., implicitly an atomic dimension below the surface.

The other two cases in Figure 6 (i.e., 6(b) and 6(c)) consider a different physical situation that is referred to as a selvedge in the gas-solid literature[22]. The selvedge in the context of electrochemical H charging can be defined as an intermediate reaction layer, more

than an atomic layer thick, having continuity with the bulk substrate. Essentially, the concept of a selvedge in this paper will be used to describe the specific subsurface region of hydrogen interaction with the metal. The situation in Figure 6(c) differs from that in Figure 6(a) only in that the hydrogen diffusivity in the selvedge is greater than that in the bulk substrate (if the hydrogen diffusivity were lower in the selvedge than in the bulk, the slope would be of the same sign but steeper than that of the bulk). The situation in Figure 6(c) might depict, for example, a surface segregated condition. In this case the intercept (c_g) of the i_∞ vs $\sqrt{i_r}$ plot will be negative.

The question still remains of the case where the intercept (c_g) of the i_∞ vs $\sqrt{i_r}$ plot is positive as in the data of Bockris $et\ al.$ (Figure 3). For a pure metal, this can only be achieved by a diffusionless process such as a situation where the hydrogen atom actually penetrates into the substrate a finite distance, l_i, (of atomic dimension) immediately after the proton discharge step. This possibility has not been ruled out on theoretical grounds and the above mentioned positive intercept in the data in Reference 2 indicates that some type of diffusionless process may be involved. If hydrogen does penetrate into the lattice driven by the energy associated with the proton discharge step, the initial hydrogen subsurface concentration profile should be similar to that obtained during ion implantation, in that a maximum in concentration occurs at some distance beneath the substrate surface where the penetrating atoms come to rest. The normal hydrogen diffusional process would commence immediately following this nondiffusional step with most of the hydrogen atoms diffusing back towards the input surface since this surface is much closer to the concentration maximum than is the other (exit) surface of the membrane. Since, during ongoing hydrogen discharge, both processes (penetration and diffusion) may occur simultaneously, the profile for steady state hydrogen permeation could be as shown in Figure 6(b). Thus, the intercept (c_g) in the i_∞ vs $\sqrt{i_r}$ plot (Figure 3) is positive.

In order to take care of the various possible cases of concentration profiles (Figure 6(b), where $c_g > O$ and Figure 6(c), where $c_g < O$) the basic I-P-Z model has to be modified slightly, as follows:

$$c_g = c_i - c_s \tag{14}$$

where c_i = the subsurface hydrogen concentration at the selvedge boundary and c_g is the concentration difference in the selvedge, which is assumed to be independent of i_c; ie.,

$$c_s = c_i - c_g \tag{14a}$$

Equation (3) will be modified as:

$$i_\infty \approx F (D_l/L) c_i \tag{14b}$$

From Equations (14a) and (14b),

$$c_s = \left(\frac{L}{FD_1}\right) i_\infty - c_g = b\, i_\infty - c_g \tag{15}$$

where $b = L/(FD_1)$.

From Equations (2), (4) and (15),

$$i_\infty = k'' \left(b\sqrt{Fk_3}\right)^{-1} \sqrt{i_r} + \left(c_g/b\right) \tag{16}$$

Similarly, using Equations (1), (4) and (15), Equation (6d) will be modified (by considering the selvedge) as:

$$i_c\, e^{a\alpha\eta} = -\left(\frac{b i_o{}'}{k''}\right) \left[i_\infty - \left(c_g/b\right)\right] + i_o{}' \tag{17}$$

Utilizing Equations (16) and (17), the data of Bockris et al.[2] can be analyzed as was done above for the other three cases. The modified plot, $i_c\, e^{a\alpha\eta}$ vs $[i_\infty - (c_g/b)]$ is shown in

Figure 7. The relevant quantities utilized for this analysis and the resulting computed

parameters are shown in Table I, alongside the results for the other three cases. It is to be

noted in Table I that the value of c_g is quite small in this case and so, neglecting the value of

c_g in calculations of the various transport and kinetic parameters would not introduce serious

errors.

A modified version of the reaction sequence used in the derivation of the basic I-P-Z

model is shown in Figure 8, where the selvedge reaction is also included.

III. The Limiting Conditions for Diffusion Control Versus Interface Control.

From Equation (4),

$$\frac{1}{c_s} = (\frac{k_{ads}}{k_{abs}\theta_s}) + (\frac{D_l}{Lk_{abs}\theta_s}) \tag{18a}$$

Substituting for c_s ($= \frac{L}{FD_l} i_\infty$) from Equation (3) into Equation (18a) and simplifying:

$$\frac{1}{i_\infty} = (\frac{Lk_{ads}}{FD_l k_{abs}\theta_s}) + (\frac{1}{Fk_{abs}\theta_s}) \tag{18b}$$

Equation (18b) describes the same relationship as derived by Kim and Wilde[10] and by

Ateya et al.[11]. As Ateya et al.[11] have pointed out, there are two important limiting cases of

Equation (18b) or equivalently Equation (4).

Case I. For thick membranes, or low values of D_l, i.e. under conditions of pure diffusion

control, $\frac{D_l}{L} \ll k_{ads}$ and hence Equation (4a) will reduce to:

$$k'' = \frac{k_{abs}}{k_{ads}} = k' \tag{19a}$$

As pointed out before, k' is usually termed as the equilibrium absorption-adsorption

constant.

It can then be easily shown that Equation (18b) reduces to:

$$\frac{1}{i_\infty} = \frac{L}{D_l}\ \frac{k_{ads}}{Fk_{abs}\theta_s} = \frac{L}{D_l}\ \frac{1}{Fk'\theta_s} \tag{19b}$$

Rearranging, one has

$$i_\infty = F\frac{D_l}{L}\ k'\ \theta_s \tag{19c}$$

Equation (19c) is a familiar relationship. In other words, the assumption of the intermediate reaction rate constant being thickness independent can be valid for thick membranes or low values of D_l.

Case II. For very thin membranes, or high values of D_l, or low values of k_{abs}, $\frac{D_l}{L} \gg k_{ads}$ and hence Equation (4a) will reduce to:

$$k'' = \frac{k_{abs}}{(\frac{D_l}{L})} \tag{20a}$$

It can then be easily shown that Equation (18b) reduces to:

$$\frac{1}{i_\infty} = \frac{1}{Fk_{abs}\theta_s} \tag{20b}$$

or

$$i_\infty = Fk_{abs}\theta_s \tag{20c}$$

Equation (20c) is the same relationship as that of Ateya *et al.*[11]. As pointed out by them, i_∞ becomes thickness independent and the hydrogen entry will be interface controlled.

IV. Evaluation of the Surface and Subsurface Kinetic Properties of a Metal Electrode Using the I-P-Z Model.

The H adsorption and absorption rate constants describe the surface and subsurface kinetics for the metal electrode. These kinetic properties could eventually be utilized to characterize the surface and subsurface states of a metal.

From Equation (4a), the following important general relationship can be obtained:

$$\frac{1}{k''} = (\frac{k_{ads}}{k_{abs}}) + (\frac{D_l}{k_{abs}}) \frac{1}{L} \tag{21}$$

The hallmark of Equation (21) is that by plotting $\frac{1}{k''}$ vs. $\frac{1}{L}$, one can obtain some of the ever-sought surface properties, such as k_{abs} and k_{ads}. If the $\frac{1}{k''}$ vs. $\frac{1}{L}$ plot is linear, then Equation (21) is applicable, which implies that the adsorbed hydrogen is the same intermediate which takes part in both the evolution and absorption steps, as has been proposed by Bockris and others[2,4,23,24] over the decades and generally accepted.

Figure 9 shows the plot of $\frac{1}{k''}$ vs. $\frac{1}{L}$ for iron data (as per Table I). It shows the correct trend, as expected from Equation (21), illustrating the validity of k" values obtained by the application of the I-P-Z model to the permeation data of various iron membranes. But it is to be noted that $\frac{1}{k''}$ vs. $\frac{1}{L}$ is not linear, even after considering the error bands. This, however, does not imply that the adsorbed and absorbed hydrogen are not the same intermediates, since impurity levels of the iron membranes as well as the electrolytes are different for the three sets of iron data and hence the k_{abs} (and even D_l) and k_{ads} values would be different.

V. Advantages of the I-P-Z Model

The I-P-Z model has the following advantages.

(1) It enables calculation of surface coverages, reaction rate constants and the potential range in which a particular reaction mechanism will occur, by utilizing i_∞ for the determination of k", etc. as noted earlier in conjunction with Equations (6a) through (6d).

(2) It is able to explain physically and mathematically all the different processes involved in a self consistent manner. Also, it is quite flexible to modifications that will take care of changing physical and chemical conditions. That is, the basic I-P-Z model will serve as a building block for more sophisticated models.

(3) The I-P-Z model in conjunction with the derivations of Ateya et al.[11], for the first time focuses on the importance of the membrane thickness and the limiting conditions for diffusion control versus interface control.

(4) It has a unique capacity to quantitatively evaluate the ever-sought surface and subsurface kinetic properties, i.e., the H adsorption and absorption rate constants.

(5) It delineates the roles of electrochemical kinetics (discharge reaction - proton tunneling), possible unique surface layer kinetics (selvedge reaction) and physico-chemical kinetics (permeation and recombination reactions). Strictly speaking, all of the rate constants (except that for the discharge reaction) should be potential independent and this model recognizes that. From these simple concepts, the model advances that the potential range in which a certain mechanism will be operating is bounded. This is true for the coupled discharge - recombination mechanism, analyzed by the model. Comparison of the various calculated rate constants help to verify the mechanism and the validity of the assumptions. These are further checked by the linearity of the two plots, i_∞ vs $\sqrt{i_r}$ and $f_{i\eta}$ vs i_∞'. In short, the model can serve as a diagnostic scheme to analyze consistency between the observed relationship and the proposed mechanism by calculating the rate constants and the critical potential ranges from the η-i_c-i_∞ data base.

(6) The model, when adequately modified, has the capacity to explain and predict the behavior of poisons, such as H_2S, enhancing permeation but in many cases decreasing the hydrogen overvoltage at a constant charging density. This will be considered in detail in an upcoming paper[8], where the model is modified by incorporating the Frumkin-Temkin correction.

VI. Limitations of the I-P-Z Model

(1) The model cannot be used in its present form when the backward reactions become important, i.e., at small hydrogen overpotentials ($\eta \lesssim RT/F$)

(2) The possibility of the occurrence of the selvedge reaction and, hence, the value of l_i have to be experimentally and theoretically investigated.

(3) The actual potential dependence of $k_{1\eta}$ (Equation (9)) as well as the proper criteria for finding the potential range in which a mechanism, such as the coupled discharge-recombination reaction operates, have to be evaluated.

Notwithstanding the above limitations of this model, it can provide some important information about surface coverages, rate constants and operating mechanism. The concept of the selvedge, if proven by specially designed experiments, has the capacity to provide a detailed physical picture for explaining many of the complex phenomena occurring during hydrogen entry and embrittlement in many materials.

CONCLUSIONS

1. A model has been developed which for the first time takes into account the effect of the hydrogen permeation flux, i_∞, on the hydrogen evolution reaction during electrochemical hydrogen charging of materials. This model gives the critically important values of the absorption (k_{abs}) and adsorption (k_{ads}) rate constants, discharge and recombination rate constants and hydrogen coverages from hydrogen permeation data. In addition, an analytical method in the model facilitates the determination of the operating mechanism of the hydrogen evolution reaction.

2. The model also incorporates the thickness and diffusivity factors of the membrane into the absorption and adsorption rate constants in order to address and compare the various electrochemical and physico-chemical reactions.

3. A few of the literature data of hydrogen permeation in iron and nickel are successfully analyzed with this model.

4. Further experiments and analyses need to be performed in order to check the validity of the assumptions, and the role, if any, of the selvedge reaction.

ACKNOWLEDGEMENT

LIST OF SYMBOLS

a a constant, F/RT, $(volts)^{-1}$

a_{H^+} hydrogen ion activity, dimensionless

a_{H_2O} activity of water in the electrolyte, dimensionless

A amperes

b a constant, L/FD_H, $(A.L)^{-1}$

c_g concentration difference in the selvedge, $c_i - c_s$, $mol\ L^{-3}$

c_{H^+} hydrogen ion concentration, 10^{-pH}, $mol\ L^{-3}$

c_i subsurface hydrogen concentration, $mol\ L^{-3}$

c_s surface hydrogen concentration, $mol\ L^{-3}$

D_i hydrogen diffusion coefficient in the selvedge (transition layer), $L^2\ s^{-1}$

D_l lattice hydrogen diffusion coefficient, $L^2\ s^{-1}$

E_{eq} equilibrium potential for the h.e.r., mV vs SHE

F Faraday constant, 96500 C $(g-eq)^{-1}$

$f_{i\eta}$ a variable, $i_c e^{a\alpha\eta}$, $A\ L^{-2}$

ΔG_i^* activation energy of reaction i, $J(g-mol)^{-1}$

i_c charging flux or current density, $A\ L^{-2}$

i_∞ steady state permeation flux, $A\ L^{-2}$

i_∞' a variable, $i_\infty - c_g/b$, $A\ L^{-2}$

i_o exchange current density, $A\ L^{-2}$

i_o' $i_o/(1-\theta_e)$, $A\ L^{-2}$

i_r steady state evolution flux, $A\ L^{-2}$

k_{abs} absorption rate constant, $mol\ (L^2 s)^{-1}$

k_{ads} adsorption rate constant, $L\ s^{-1}$

k' equilibrium absorption-adsorption constant, $mol\ L^{-3}$

k'' thickness dependent absorption-adsorption constant, $mol\ L^{-3}$

k_1^o discharge reaction rate constant, $mol\ (L^2 s)^{-1}$

k_1 discharge reaction rate coefficient, mol $(L^2 s)^{-1}$

$k_{1\eta}$ potential dependent discharge reaction rate coefficient, mol $(L^2 s)^{-1}$

k_2 selvedge (intermediate) reaction rate constant, $L\,s^{-1}$

k_{-2} reverse (intermediate) reaction rate constant, $L\,s^{-1}$

k_3 recombination reaction rate constant, mol $(L^2 s)^{-1}$

L membrane thickness, L

L unit length

l_i selvedge depth, L

R gas constant, 8.314 J $(g\text{-mol K})^{-1}$

s_c slope of $\ln(i_c)$ vs η, decade V^{-1}

s_{ct} slope of η vs log i_c, V decade^{-1}

s_∞ slope of $\ln(i_\infty)$ vs η, decade V^{-1}

$s_{\infty t}$ slope of η vs log i_∞, V decade^{-1}

T temperature, K

Greek Symbols

α	transfer coefficient, dimensionless
η	overvoltage, V
η_c	cathodic overvoltage, V
η_c^l	lower limit of η_c, V
η_c^u	upper limit of η_c, V
θ_s	surface coverage, dimensionless
θ_e	equilibrium surface coverage, dimensionless
γ	gradient of the apparent standard free energy of adsorption with hydrogen coverage, $J\ (g\text{-mol})^{-1}$

REFERENCES

1. M.A. Devanathan and L. Stachurski, J. Electrochem. Soc. Vol. 111, p.619 (1964).

2. J, O'M. Bockris, J. McBreen and L. Nanis, J. Electrochem. Soc. Vol. 112, p. 1025 (1965).

3. C. Kato, H.J. Grabke, B. Egert and G. Panzner, Cor. Sci. Vol. 24, No. 7, p. 591 (1984).

4. J. McBreen and M. A. Genshaw: Fundamental Aspects of Stress Corrosion Cracking (Conf. Proc.), R.W. Staehle, et. al., eds., NACE-1 (1969), p. 51.

5. L. Nanis and T.K.G. Namboodhiri.: SCC and HE of iron base alloys (Conf. Proc.), R.W. Staehle et al eds., NACE-5 (1977), p. 432.

6. M. Zamanzadeh, A. Allam, H. W. Pickering and G. K. Hubler, J. Electrochem. Soc., Vol. 127, p. 1688 (1980).

7. M. Zamanzadeh, A. Allam, C. Kato, B. Ateya and H.W. Pickering, J. Electrochem. Soc. Vol. 129, p.284 (1982).

8. R.N. Iyer, I. Takeuchi, M. Zamanzadeh and H.W. Pickering, "Hydrogen Sulfide Effect on Hydrogen Entry into Iron - A Mechanistic Study" (in preparation for publication in Corrosion Journal).

9. E. G. Dafft, K. Bohnenkamp and H.J. Engell, Corrosion Science, Vol. 19, p. 591 (1979).

10. C. D. Kim and B. E. Wilde, J. Electrochem. Soc., Vol. 118, p. 202 (1971).

11. B. G. Ateya and H. E. Abd Elal: Corrosion - Industrial Problems, Treatment and Control Techniques (Conf. Proc.), V. Ashworth ed., KFAS Proc. Series, Vol. 2 (1984), Pergamon Press, p. 201.

12. J. O'M Bockris and A.K.N. Reddy: Modern Electrochemistry, Vol. 2, A Plenum/Rosetta Edition, Plenum Press, N.Y. (1970), pp. 1235, 959-975.

13. E. Gileadi and B.E. Conway, Modern Aspects of Electrochemistry, No. 3, J. O'M. Bockris and B.E. Conway, eds., Butterworths, Washington (1964) pp. 347 - 442.

14. R. N. Iyer, H. W. Pickering and M. Zamanzadeh, Scripta Metallurgica, Vol. 22, p. 911 (1988).

15. M. Smialowski: Hydrogen in steel, Addison-Wesley, Reading, Massachusetts (1962), p. 141.

16. J. O'M. Bockris and P. K. Subramanyan, J. Electrochem. Soc., Vol. 118, p. 1114 (1971).

17. J. O'M. Bockris and P. K. Subramanyan, Electrochim. Acta, Vol. 16, p. 2169 (1971).

18. R.M. Latanision and M. Kurkela, Corrosion, Vol. 39, No. 5, p. 174 (1983).

19. J. Neter, W. Wasserman and M. H. Kutner: Applied Linear Statistical Model, 2nd Edition, Richard Irwin, Inc. (1985), pp. 1-146.

20. R. A. Oriani, Fundamental Aspects of Stress Corrosion Cracking (Conf. Proc.), R. W. Staehle, et. al., eds., NACE-1 (1969), p.32.

21. H. Flitt and J. O'M. Bockris, Intern, J. of Hydrogen Energy, Vol. 7, p. 411 (1982).

22. M. Lagues and J. L. Domange, Surface Science, Vol. 47, p. 77 (1975).

23. L. Nanis: Environment-Sensitive Fracture of Engineering Materials (Conf. Proc.), Z.A. Foroulis, ed., TMS-AIME, New York (1977), p. 361.

24. R. D. McCright, ref. 5, p. 306.

APPENDIX

Determination of the Transfer Coefficient, α:

In previous determinations of α, θ_s was assumed to be close to zero and neglected which resulted in the familiar relationship between α and the Tafel slope ($\dfrac{d\eta}{d \log i_c}$)= $\dfrac{2.3\,RT}{\alpha F}$. However, in keeping with the thrust of this paper, i.e., taking into account the important effect of θ_s which is potential dependent, α needs to be rigorously derived as follows. Equation (6c), in the text, can be rewritten as:

$$i_\infty = - \left[\frac{k''}{(bi_o')} \right] i_c\, e^{a\alpha\eta} + (k'/b) \tag{A.1}$$

Differentiating Equation (A.1) with respect to the overpotential, η, (assuming α and k" are independent of η) one obtains

$$(di_\infty/d\eta) = -\left(k''/(bi_o')\right) \left[a\alpha i_c e^{a\alpha\eta} + e^{a\alpha\eta}\,(di_c/d\eta) \right] \tag{A.2}$$

and

$$\left(d^2 i_\infty/d\eta^2\right) = - \left(k''/(bi_o')\right)e^{a\alpha\eta}\left[\left(d^2 i_c/d\eta^2\right) + 2a\alpha(di_c/d\eta) + (a\alpha)^2 i_c \right] \tag{A.3}$$

Dividing Equation (A.3) by Equation (A.2), and simplifying, one obtains

$$\alpha^2 + (\alpha/a)\left[-\left\{ \left(d^2 i_\infty/d\eta^2\right)/(di_\infty/d\eta) \right\} + \left\{ (2/i_c)(di_c/d\eta) \right\} \right] +$$

$$(1/a^2)\left[(1/i_c)\left(d^2 i_c/d\eta^2\right) - (1/i_c)(di_c/d\eta)\left\{ \left(d^2 i_\infty/d\eta^2\right)/(di_\infty/d\eta) \right\} \right] = 0 \tag{A.4}$$

From plots of i_c vs η and i_∞ vs η, the above differentials (in Equation (A.4)) can be determined and then the quadratic equation in α can be solved. If the measured $\ln(i_c)$ vs η

and $\ln(i_\infty)$ vs η plots are linear, this confirms that α is independent of η, and Equation (A.4) can be simplified as:

$$\alpha^2 + \left((2s_c - s_\infty)/a\right)\alpha + \left(s_c(s_c - s_\infty)/a^2\right) = 0 \qquad (A.5)$$

where $s_c = d\ln(i_c)/d\eta$ and $s_\infty = d\ln(i_\infty)/d\eta$. The proper value of α is chosen from the solution of Equation (A.5) so as to obtain non-negative values of i_0' and k'' in Equation (A.1).

TABLE I

Analysis of Literature Data (References as shown)

Parameter	Value			
	Ref[3]	Ref[6]	Ref[18]	Ref[2]
Material	Pure Fe	Ferrovac Fe	Zone-refined Ni	Armco Fe
D_l (cm^2 s^{-1})	5×10^{-5}	5×10^{-5}	4×10^{-10}	5×10^{-5}
L (mm)	2	0.37	0.08	0.77
b (mole(A$\cdot$cm^{-1}))	0.04	0.01	200	0.02
pH	1	13	1.3	1
α	0.38	0.45	0.56	0.56
$i_0 \cong i_0'$(A cm^{-2})	3×10^{-6}	1×10^{-6}	4×10^{-6}	6×10^{-7}
k_1^O (cm s^{-1})	1×10^{-7}	0.2	2×10^{-7}	2×10^{-8}
k_1 (mole (cm^2·s)$^{-1}$)	4×10^{-11}	1×10^{-11}	4×10^{-11}	6×10^{-12}
k_3 (mole (cm^2·s)$^{-1}$)	3×10^{-6}	1×10^{-7}	5×10^{-6}	7×10^{-11}
k'' (mole cm^{-3})	2×10^{-6}	2×10^{-7}	8×10^{-3}	1×10^{-6}
c_g (mole cm^{-3})				4×10^{-8}
θ_e	0.004	0.01	0.003	0.003
η_c^l (mV)	-610	-380	-440	-430
η_c^u (mV)	-920	-640	-650	-640

FIGURE CAPTIONS

1. Various current-potential data for the hydrogen evolution reaction on iron and nickel electrodes.

2. Various hydrogen permeation data for hydrogen charging of the iron and nickel electrodes in Fig. 1.

3. Plots of the hydrogen permeation current versus square root of the recombination current.

4. Plots of the hydrogen charging function ($i_c e^{a\propto\eta}$) versus the steady state hydrogen permeation (i_∞), for iron at pH 1, iron at pH 13 and nickel at pH 1.3.

5. Plots of the fractional hydrogen coverage (θ_s) as a function of the overpotential (η) obtained by application of the model to the data. (a) η vs θ_s. (b) η vs log θ_s.

6. Sketches of the three different cases of H concentration profiles, expected for a general (physical) intermediate reaction.

7. Plot of the hydrogen charging function ($i_c e^{a\alpha\eta}$) versus the hydrogen permeation function ($i_\infty - c_g/b$), for iron at pH1.

8. Schematic showing hydrogen discharge, recombination, permeation and selvedge reactions, specifically for the case of Fig. 6(b).

9. Plot of the absorption-adsorption constant (k'') as a function of the membrane thickness (L) for various data on iron.
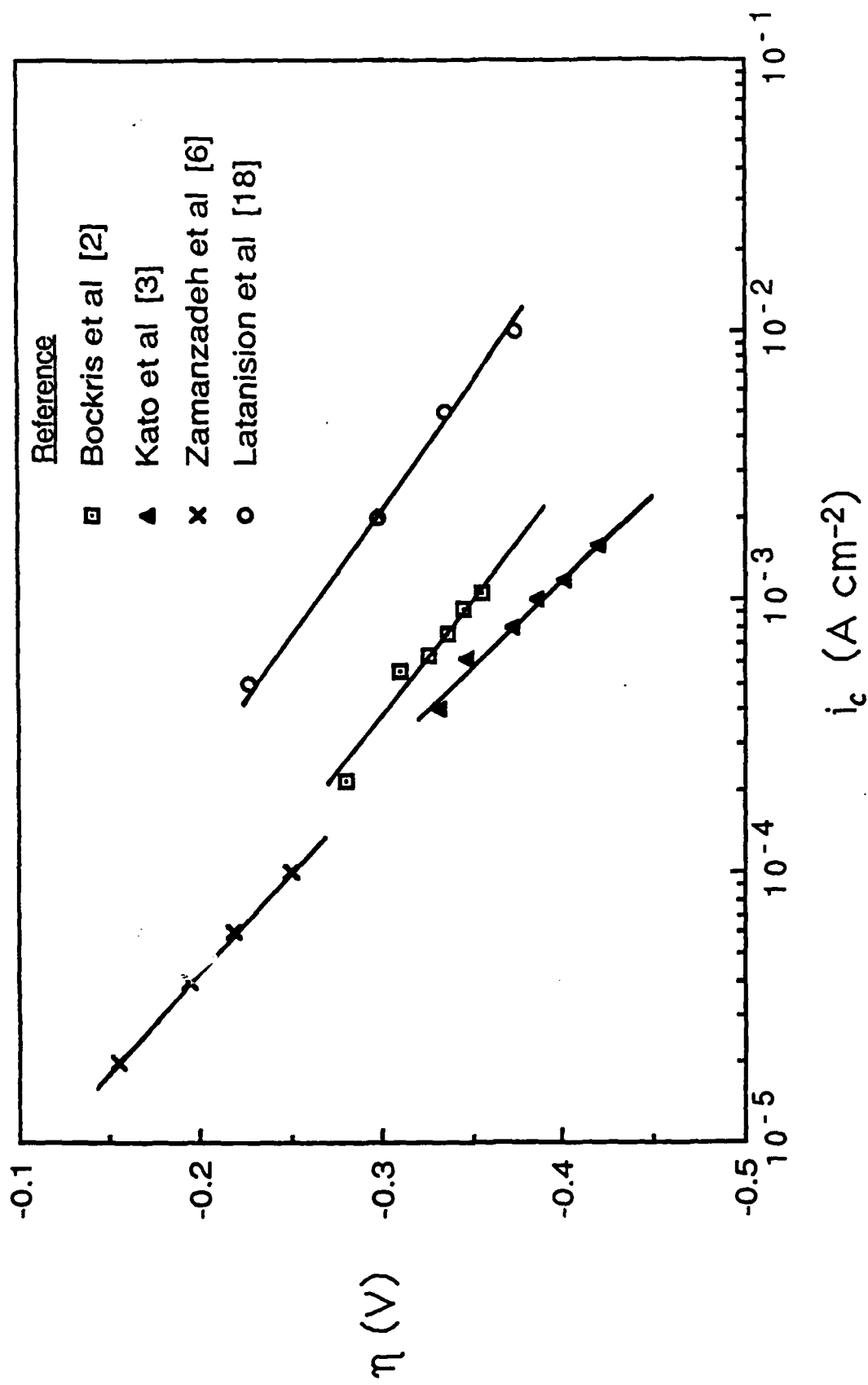
FIGURE 1., IYER, PICKERING, & ZAMANZADEH
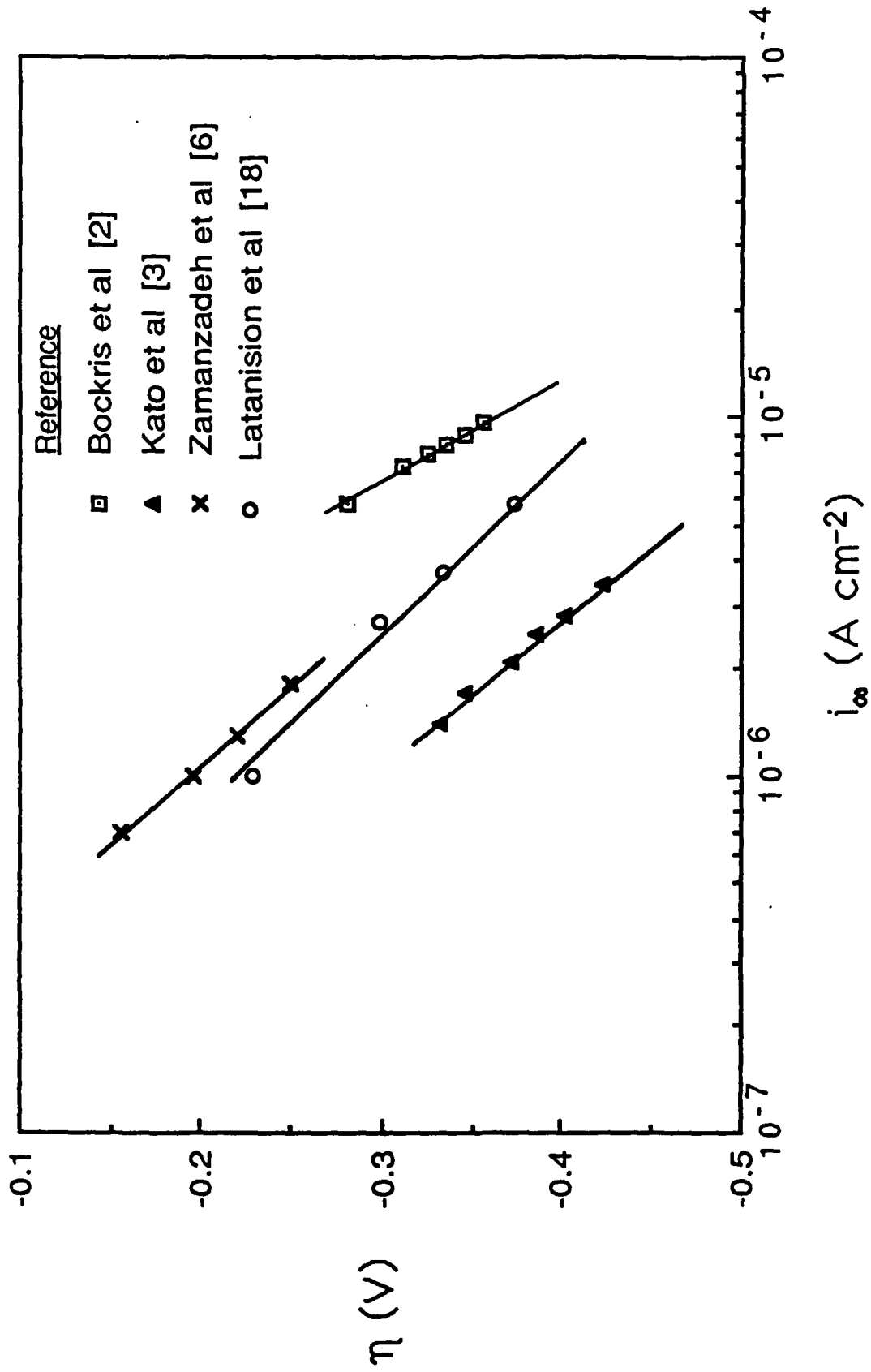
FIGURE 2., IYER, PICKERING & ZAMANZADEH
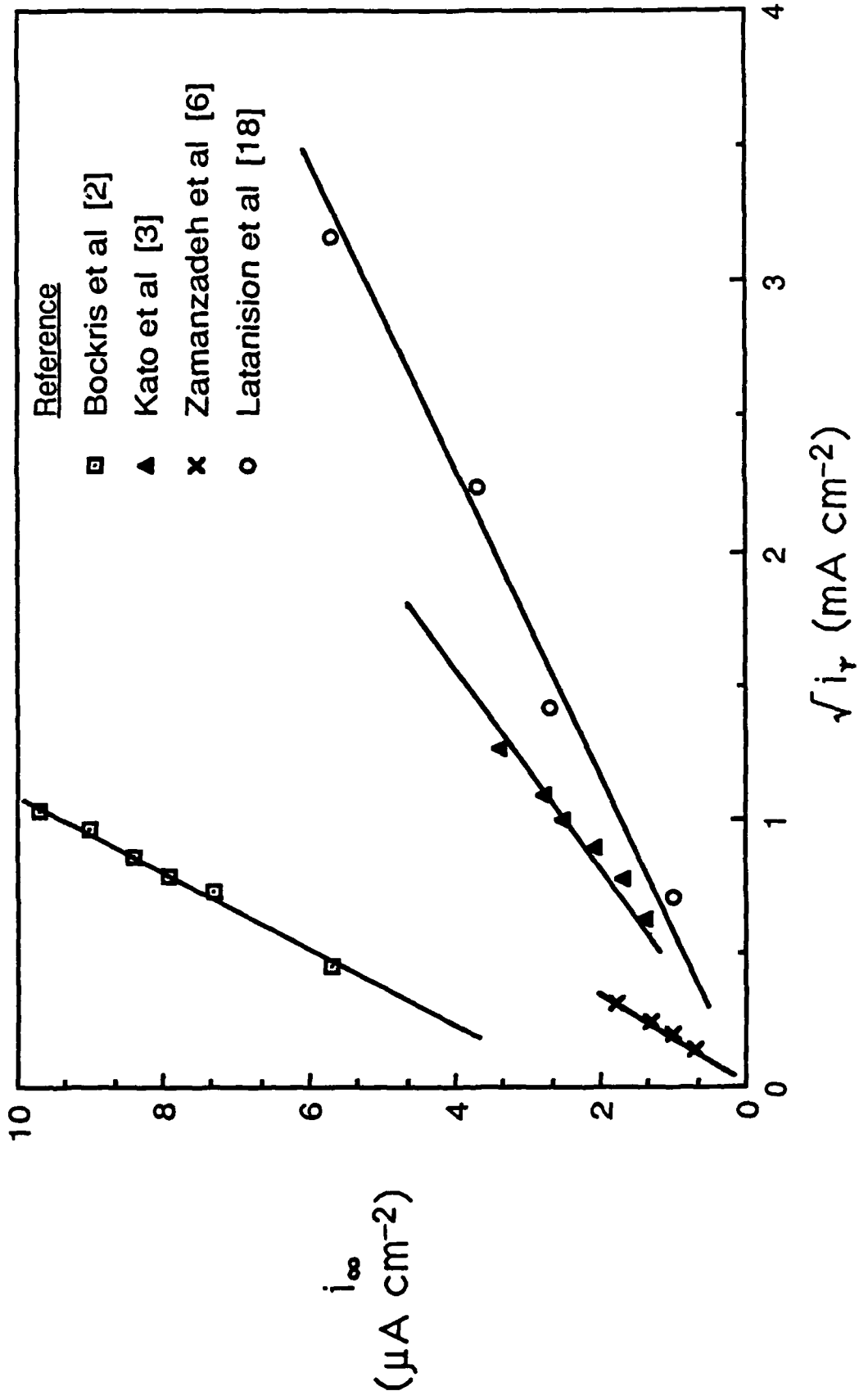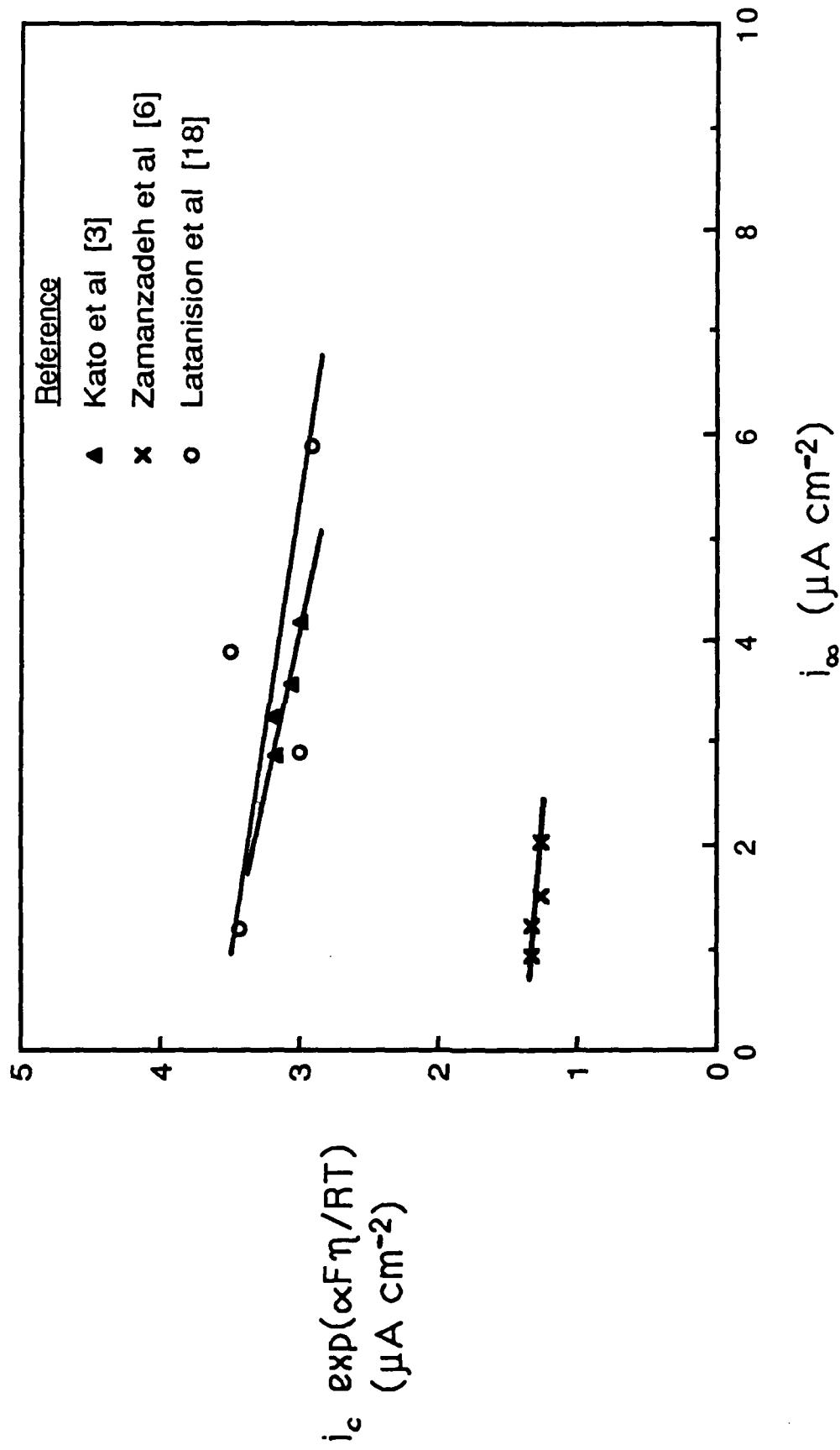
Reference

□ Bockris et al [2]
▲ Kato et al [3]
✕ Zamanzadeh et al [6]
○ Latanision et al [18]

FIGURE 3., IYER, PICKERING 'A ZAMANZADEH

Figure 4) ... Pickering v. Temperature

FIGURE 5a.) IYER, PICKERING, & ZAMANZADEH

Reference

□ Bockris et al [2]
▲ Kato et al [3]
✕ Zamanzadeh et al [6]
○ Latanision et al [18]

η (V)

$\log (\theta_s)$

-0.0
-0.1
-0.2
-0.3
-0.4
-0.5

10^{-2}
10^{-1}
10^0
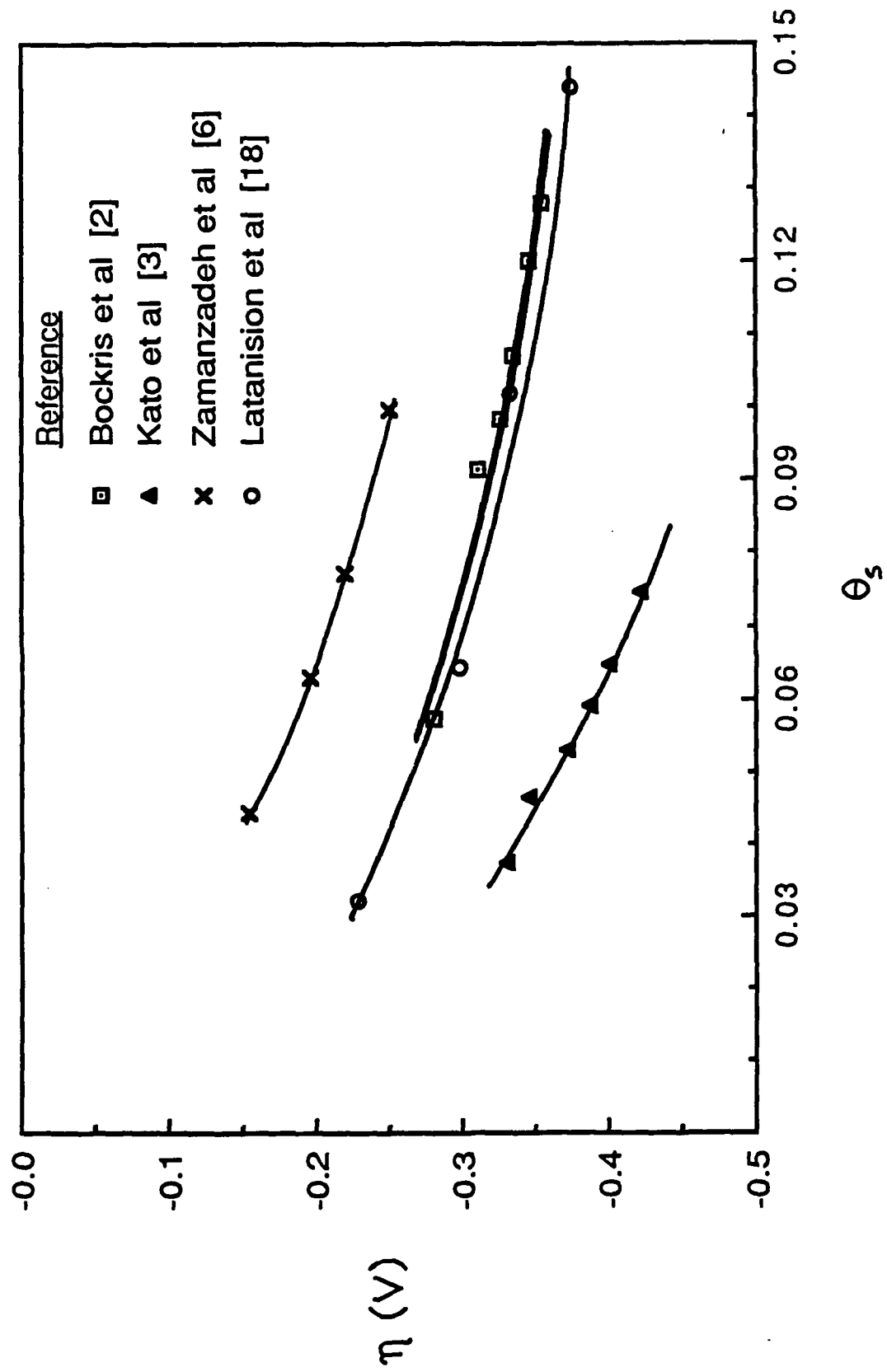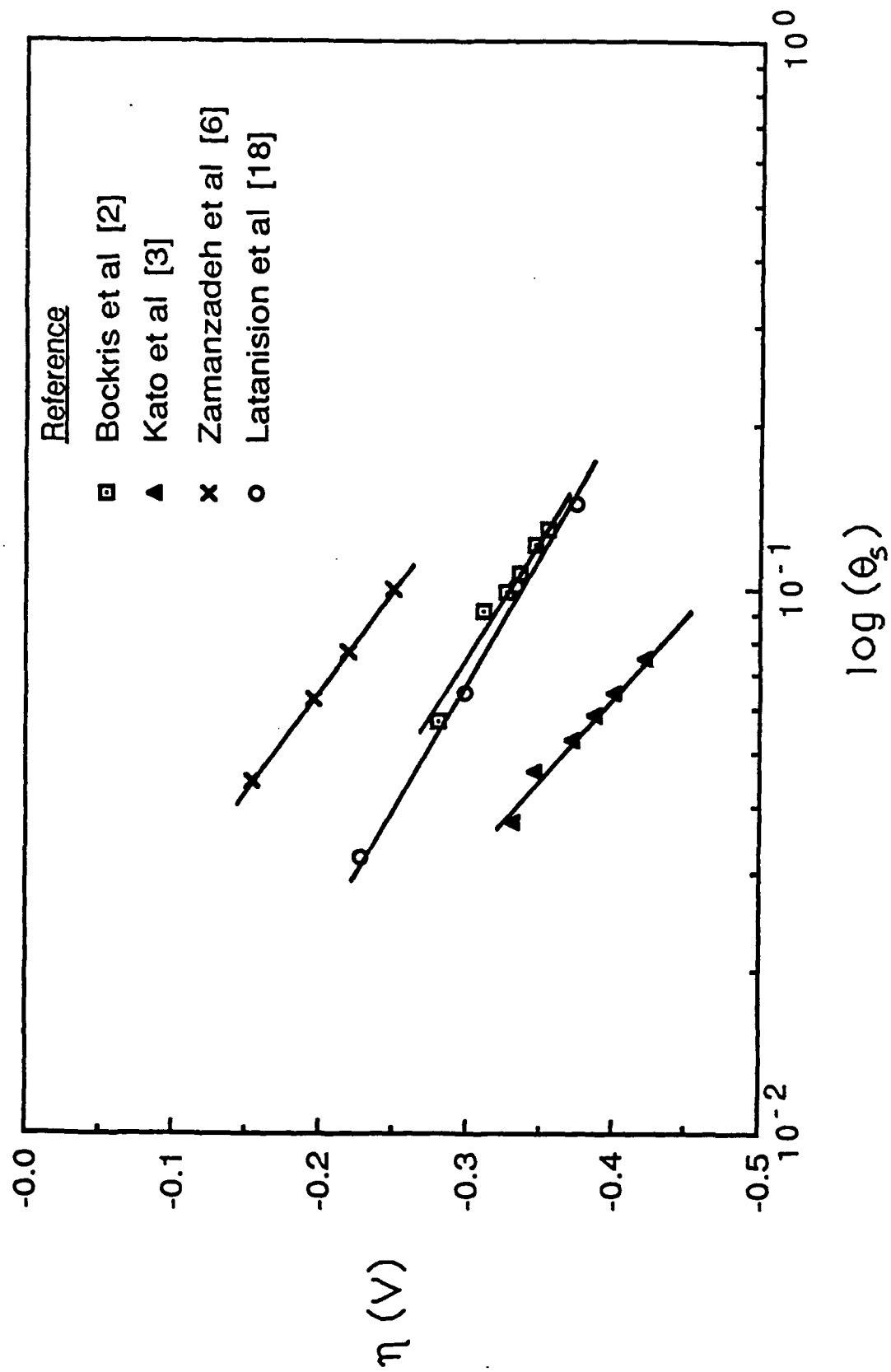
FIGURE 5 b.) IYER, PICKERING & ZAMANZADEH

(a)

(b)

(c)

FIG 6., IYER, PICKERING & ZAHNIZALEL

$i_c \exp(\alpha F\eta/RT)$ $(\mu A\ cm^{-2})$

$i_\infty - c_g/b$ $(\mu A\ cm^{-2})$

Reference

□ Bockris et al [2]
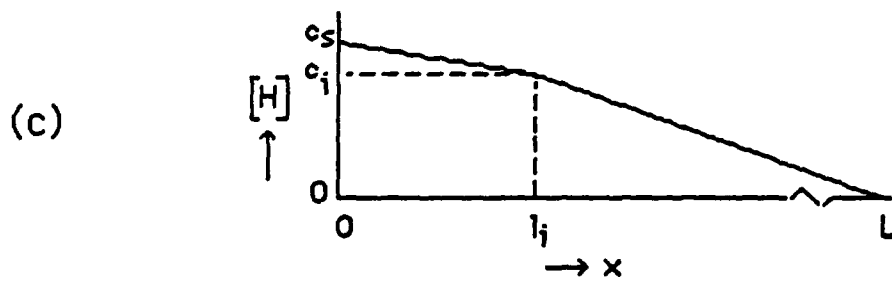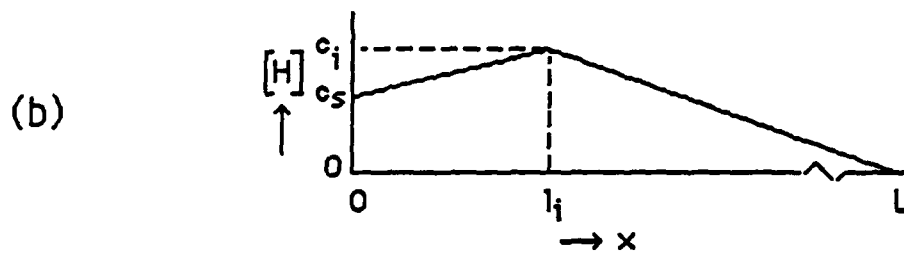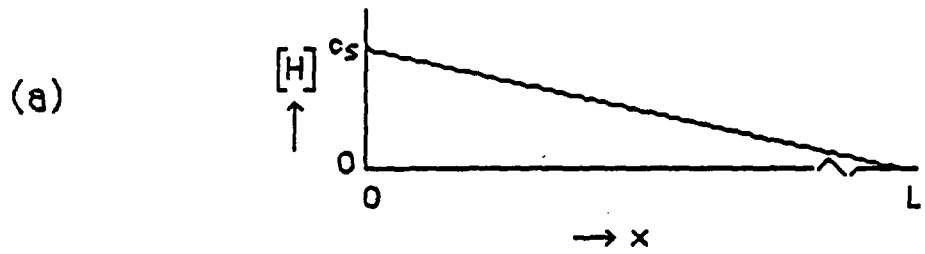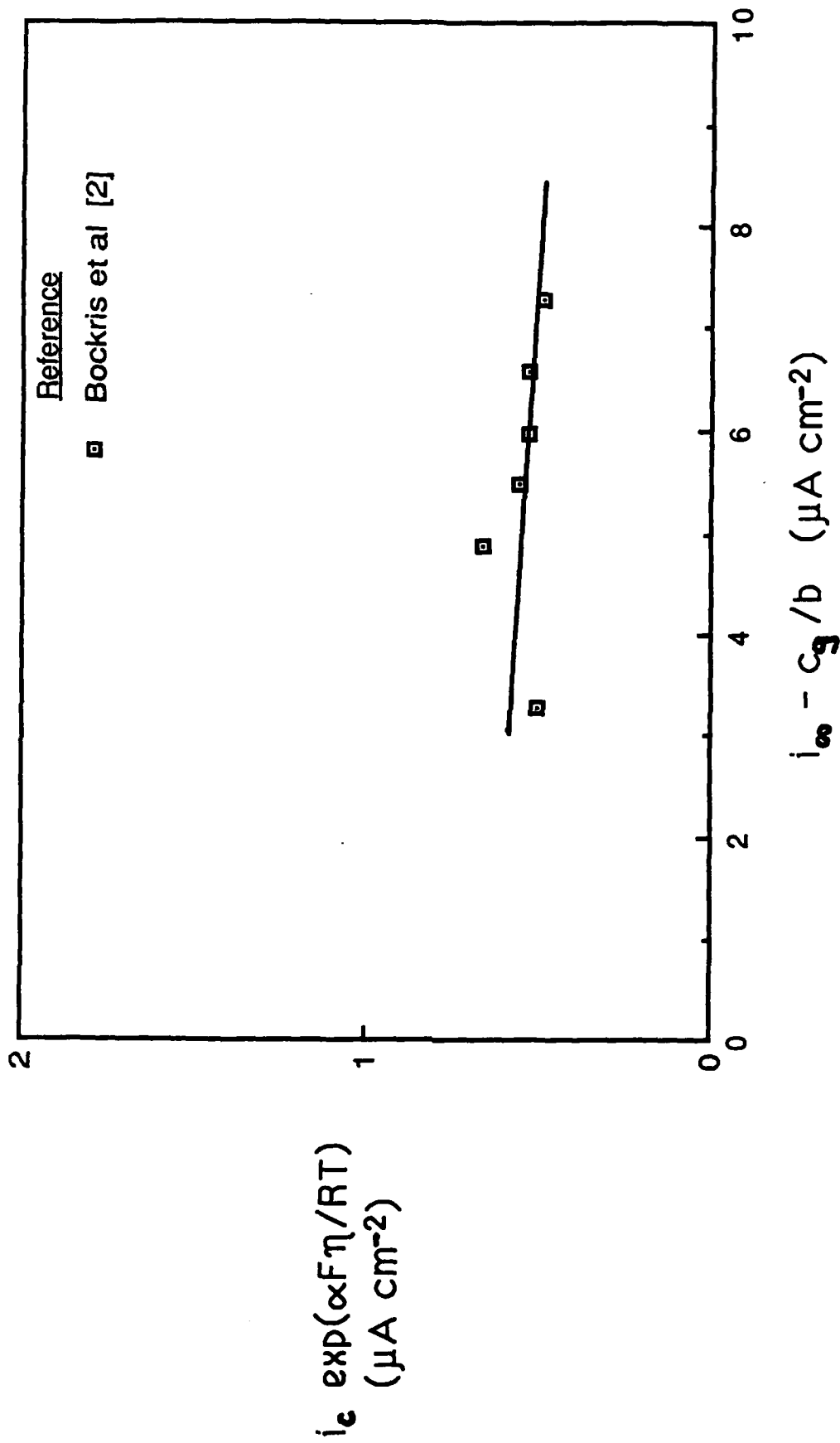
FIGURE 7.) IYER, PICKERING, & ZAMANZADEH

Cathodic Cell

$H_3O^+ + e^- \xrightarrow{\text{(1) } k_1}$

$H_2 \xleftarrow{\text{(3) } k_3}$

Selvedge

$\xrightarrow{\text{(2a) } k_2}$ $\xleftarrow{\text{(2b) } k_{-2}}$

H_{abs}

Bulk

$\xrightarrow{\text{(4) } k_4 \text{ diffusion}}$

$H \longrightarrow H^+ + e^-$

Anodic Cell

Surface $(x=0)$

Subsurface $(x=l_i)$

exit side $(x=L)$

Metal Membrane
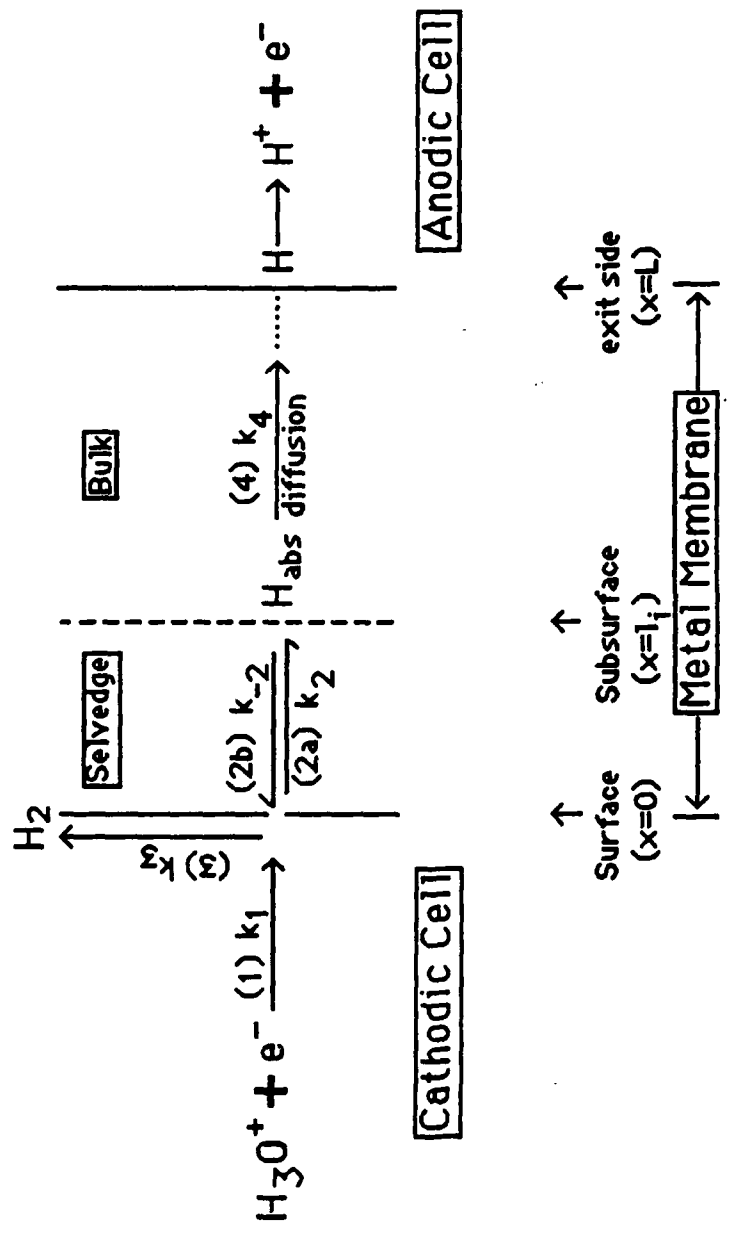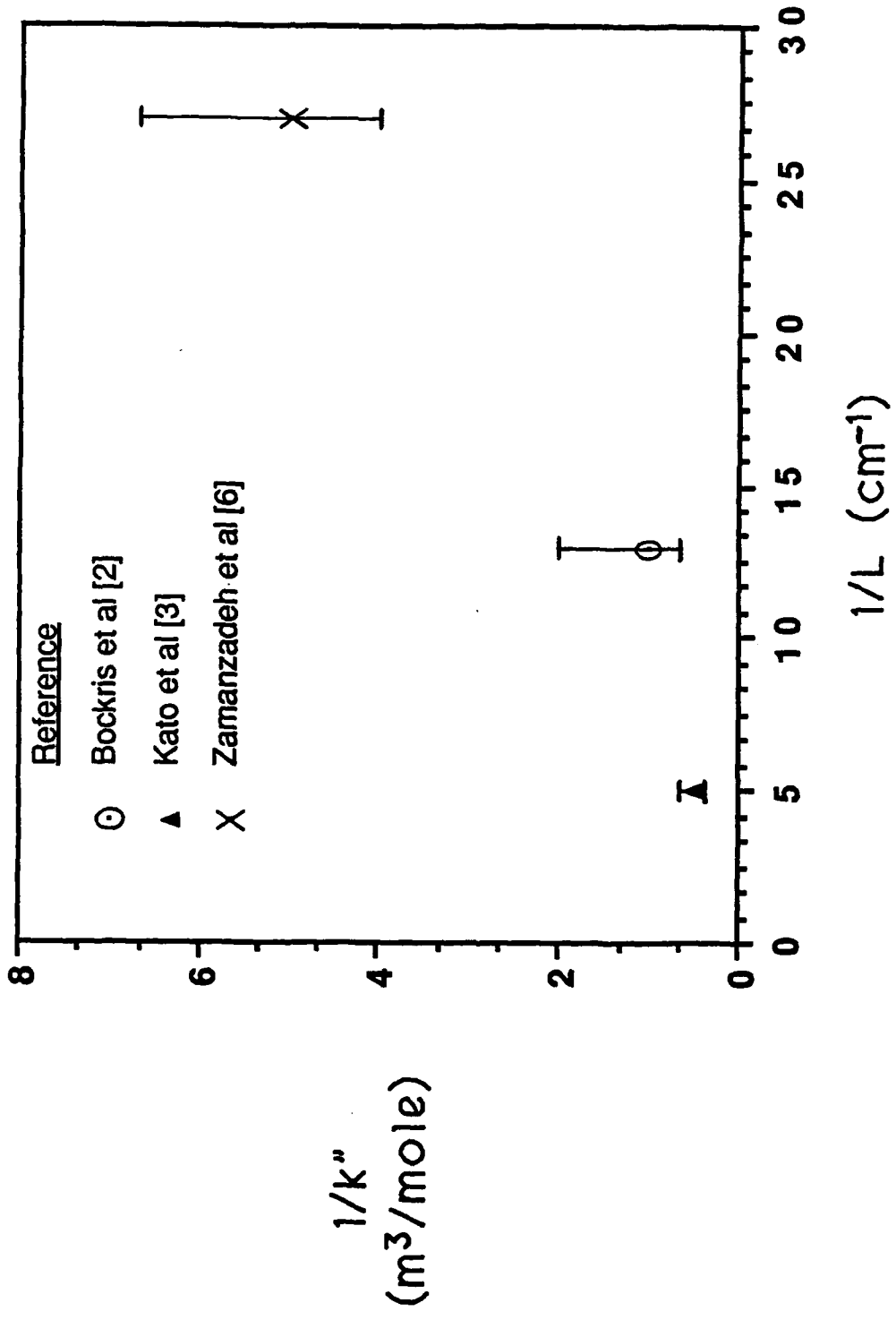
FIGURE 9) TSER, PICKERING & ZAMANZADEH

BASIC DISTRIBUTION LIST

Technical and Summary Reports   1988

Organization	Copies	Organization	Copies
Defense Documentation Center Camerson Station Alexandria, VA 22314	12	Naval Air Prop. Test Ctr. Trenton, NY 08628 ATTN: Library	1
Office of Naval Research Dept. of the Navy 800 N. Quincy Street Arlington, VA 22217 Attn: Code 1131	3	Naval Contruction Battallion Civil Engineering Laboratory Port Hueneme, CA 93043 ATTN: Materials Div.	1
Naval Research Laboratory Washington, DC 20375 ATTN: Codes 6000 6300 2627		Naval Electronics Laboratory San Diego, CA 92152 ATTN: Electron Materials Sciences Division	1
Naval Air Development Center Code 606 Warminister, PA 18974 ATTN: Dr. J. DeLuccia		Naval Missile Center Materials Consultant Code 3312-1 Point Mugu, CA 92041	1
Commanding Officer Naval Surface Weapons Center White Oak Laboratory Silver Spring, MD 20910 ATTN: Library	1	Commander David Taylor Research Center Bethesda, MD 20084	1
Naval Oceans Systems Center San Diego, CA 92132 ATTN: Library	1	Naval Underwater System Ctr. Newport, RI 02840 ATTN: Library	1
Naval Postgraduate School Monterey, CA 93940 ATTN: Mechanical Engineering Department	1	Naval Weapons Center China Lake, CA 93555 ATTN: Library	1
Naval Air Systems Command Washington, DC 20360 Attn: Code 310A Code 5304B Code 931A	1 1 1	NASA Lewis Research Center 21000 Brookpark Road Cleveland, OH 44135 ATTN: Library	1
Naval Sea System Command Washington, DC 20362 ATTN: Code 05M Code 05R	1 1	National Bureau of Standards Gaithersburg, MD 20899 Attn: Metallurgy Division Ceramics Division Fracture & Deformation Division	1 1 1

Naval Facilities Engineering
Command
Alexandria, VA 22331
ATTN: Code 03   1

Scientific Advisor
Commandant of the Marine Corps
Washington, DC 20380
ATTN: Code AX   1

Army Research Office
P.O. Box 12211
Research Triangle Park, NC 27709
ATTN: Metallurgy & Ceramics
           Program   1

Army Materials and Mechanics
Research Center
Watertown, MA 02172
ATTN: Research Programs Office   1

Air Force Office of Scientific
Research/NE
Building 410
Bolling Air Force Base
Washington, DC 20332
ATTN: Electronics & Materials
           Science Directorate   1

NASA Headquarters
Washington, DC   20546
Attn: Code RM   1

Defense Metals & Ceramics
Information Center
Battelle Memorial Inst.
505 King Avenue
Columbus, OH 43201   1

Metals and Ceramics Div.
Oak Ridge National Laboratory
P.O. Box X
Oak Ridge, TN 37380   1

Los Alamos Scientific Lab.
P.O. Box 1663
Los Alamos, NM 87544
ATTN: Report Librarian   1

Argonne National Laboratory
Metallurgy Division
P.O. Box 229
Lemont, IL 60439   1

Brookhaven National Laboratory
Technical Information Division
Upton, Long Island
New York 11973
Attn: Research Library   1

Lawrence Radiation Lab.
Library
Building 50, Room 134
Berkely, CA   1

David Taylor Research Ctr
Annapolis, MD 21402-5067
ATTN: Code 281   1
          Code 2813   1
          Code 0115   1

Supplemental Distribution List   Feb 1988

Prof. I.M. Bernstein
Illinois Institute of Technology
IIT Center
Chicago, Ill 60615

Prof. H.K. Birnbaum
Dept. of Metallurgy & Mining Eng.
University of Illinois
Urbana, Ill 61801

Prof. H.W. Pickering
Dept. of Materials Science and Eng.
The Pennsylvania State University
University Park, PA 16802

Prof. D.J. Duquette
Dept. of Metallurgical Eng.
Rensselaer Polytechnic Inst.
Troy, NY 12181

Prof. J.P. Hirth
Dept. of Metallurgical Eng.
The Ohio State University
116 West 19th Avenue
Columbus, OH 43210-1179

Prof. H. Leidheiser, Jr.
Center for Coatings and Surface Research
Sinclair Laboratory, Bld. No. 7
Lehigh University
Bethlehem, PA 18015

Dr. M. Kendig
Rockwell International Science Center
1049 Camino Dos Rios
P.O. Box 1085
Thousand Oaks, CA 91360

Prof. R. A. Rapp
Dept. of Metallurgical Eng.
The Ohio State University
116 West 19th Avenue
Columbus, OH 43210-1179

Profs. G.H. Meier and F.S.Pettit
Dept. of Metallurgical and
Materials Eng.
University of Pittsburgh
Pittsburgh, PA 15261

Dr. W. C. Moshier
Martin Marietta Laboratories
1450 South Rolling Rd.
Baltimore, MD 21227-3898

Prof. P.J. Moran
Dept. of Materials Science & Eng.
The Johns Hopkins University
Baltimore, MD 21218

Prof. J. Kruger
Dept. of Materials Science & Eng.
The Johns Hopkins University
Baltimore, MD 21218

Prof. R.P. Wei
Dept. of Mechanical Engineering
and Mechanics
Lehigh University
Bethlehem, PA 18015

Prof. W.H. Hartt
Department of Ocean Engineering
Florida Atlantic University
Boca Raton, Florida 33431

Dr. B.G. Pound
SRI International
333 Ravenswood Ave.
Menlo Park, CA 94025

Prof. C.R. Clayton
Department of Materials Science
& Engineering
State University of New York
Stony Brook
Long Island, New York 11794

Prof. Boris D. Cahan
Dept. of Chemistry
Case Western Reserve Univ.
Cleveland, Ohio   44106

Dr. K. Sadananda
Code 6323
Naval Research Laboratory
Washington, D.C.   20375

Prof. M.E. Orazem
Dept. of Chemical Engineering
University of Virginia
Charlottesville, VA   22901

Dr. G.R. Yoder
Code 6384
Naval Research Laboratory
Washington, D.C.   20375

Dr. N. S. Bornstein
United Technologies Research Center
East Hartford, CT   06108

Dr. A.L. Moran
Code 2812
David Taylor Research Center
Annapolis, MD   21402-5067

Dr. B.E. Wilde
Dept. of Metallurgical Engineering
The Ohio State University
116 West 19th Avenue
Columbus, OH   43210-1179

Prof. G.R. St. Pierre
Dept. of Metallurgical Eng.
The Ohio State University
116 West 19th Avenue
Columbus, OH   43210-1179

Prof. G. Simkovich
Dept. of Materials Science & Eng.
The Pennsylvania State University
University Park, PA   16802

Dr. E. McCafferty
Code 6322
Naval Research Laboratory
Washington, D. C.   20375

Dr. J.A. Sprague
Code 4672
Naval Research Laboratory
Washington, D.C.   20375

Dr. C.M. Gilmore
The George Washington University
School of Engineering & Applied
 Science
Washington, D.C.   20052

Dr. F.B. Mansfeld
Dept. of Materials Science
University of Southern California
University Park
Los Angeles, CA   90089

Dr. Ulrich Stimming
Dept. of Chemical Eng. & Applied
 Chemistry
Columbia University
New York, N.Y.   10027

Prof. J. O'M. Bockris
Dept. of Chemistry
Texas A & M University
College Station, TX   77843